



Adsorption and Photocatalytic degradation of crystal violet dye in the presence of different metals doping on TiO₂

Ayad F. Alkaim^{1*}, Mohammed B. Alqaraguly¹

^{1*}Department of Chemistry, Faculty of Girls Science, Babylon University, Hilla, Iraq.

Email: ayad_alkaim@yahoo.com

Received on 08th March and finalized on 11th March 2013.

ABSTRACT

In this work, titanium dioxide particles TiO₂ (Hombikat UV 100) doped with 0.5 % of Pt, Rh and Ru metals. They are prepared by photodeposition method. The bare TiO₂ and prepared samples were characterized by powder X-ray diffraction (XRD), UV–VIS diffuse reflectance spectra (UV–VIS, DRS), nitrogen adsorption BET, and atomic force microscopy (AFM). XRD data shows that the most particles with a size less than 10 nm. While AFM shows most particles with a size more than (55-65 nm). The band gap energy values for bare TiO₂, Pt/TiO₂, Pd/TiO₂, Rh/TiO₂ and Ru/TiO₂ were calculated by using the Kubelka-Munk model. The results show that, the band gap values were decreased with metalized TiO₂ and obtained a red shift. This in agreement with the values decreasing of crystallite size, average diameter (particle size) and surface area. The adsorption and photocatalytic degradation of CV dye over bare TiO₂, Pt/TiO₂, Pd/TiO₂, Rh/TiO₂ and Ru/TiO₂, has been studied. The addition of Pd or Pt dramatically increases the adsorption and photocatalytic degradation of CV dye. On the contrary, the Rh doped TiO₂ is far less active, while Ru doped TiO₂ decrease the photocatalytic activity of CV. It was found that the photocatalytic degradation activity of crystal violet showed the following trend: Pt/TiO₂ ≈ Pd/TiO₂ > Rh/TiO₂ > TiO₂ > Ru/TiO₂.

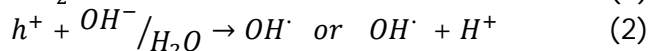
Keywords: Adsorption, Photocatalytic degradation, TiO₂, Pt/TiO₂, Pd/TiO₂, Rh/TiO₂, Ru/TiO₂.

INTRODUCTION

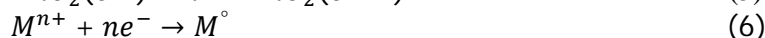
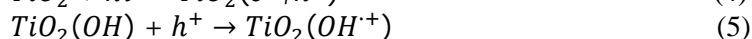
Organic dyes are generally present in the industrial wastewaters, which cannot be easily degraded, resulting in potentially environmental problems[1]. The release of those colored wastewaters in the environment is a considerable source of nonesthetic pollution and lead to originate dangerous byproducts through different sources such as oxidation, hydrolysis or other chemical reactions taking place in the wastewater phase[2]. Crystal violet is a well-known dye and has been used for various purposes (such as a biological stain, a dermatological agent, a veterinary medicine, an additive to poultry feed to inhibit propagation of mold, intestinal parasites and widely used as a purple dye for textiles such as cotton and silk, and in paints and printing ink.[3] Also it is harmful by inhalation, ingestion, through skin contact and has also been found to cause cancer, severe eye irritation in human beings[4]. Several solutions are proposed for removal of these industrial wastewaters, including adsorption[3], chemical oxidation[5], catalytic wet oxidation[6] and biological [7]. During the past decade, great interest has been focused on a promising technology based on the oxidation of the crystal violet dye, by the use of advanced oxidation

processes (AOPs)[8-11], semiconductor photocatalysis has become an increasingly promising technology in environmental wastewater treatment[12]. Among the semiconductors favorable for heterogeneous photocatalysis, TiO₂ has been most widely used due to its multiple suitable properties, such as crystalline structure, band-gap energy, photocorrosion stability, inertness, safety and cost[13].

The mechanism of the UV/TiO₂ process has been discussed extensively in the literature [14, 15]. When TiO₂ is irradiated with light energy equal to or higher than its band-gap, an electron (e⁻) can be promoted from the valence band to the conduction band and leaving a hole (h⁺) in the valence band



In aqueous phase, the photo-induced h⁺ is apparently capable to oxidize surface hydroxyl groups or surface-bond water-molecules to produce nonselective and highly reactive hydroxyl radicals (OH[·]) (2). The OH[·] radicals are considered to be the dominant oxidizing species contributing to the photocatalytic degradation of organic substrates[16]. Nevertheless, the e⁻ can recombine with the h⁺ (3), causing a decrease in the availability of the photoinduced h⁺ [17]. Therefore significant enhancements in photocatalytic activity have been reported in TiO₂ materials modified by the surface deposition of metals [18]. The presence of a metal at the surface of TiO₂ results in the formation of a Schottky barrier at the metal-semiconductor interface, which facilitates the interfacial electron transfer and subsequently encourages the charge carrier separation and can trap the photo-generated electrons efficiently[19]. This process of metal doping is described by the series of reactions (4)–(6). Depending on the preparation conditions, this photo-deposition procedure typically yields small metal[20].



Where Mⁿ⁺ is metal ion doped.

In the present work adsorption and photocatalytic degradation of Crystal violet using UV light and the metals ions "Pt, Pd, Rh, and Ru" doped TiO₂ have been studied. Very few researches have been found for comparative of photocatalytic degradation of crystal violet in the presence of metal loaded TiO₂ [9].

MATERIALS AND METHODS

Materials: Titanium dioxide UV100 is commercially available and can be obtained from (Sachtleben Chemie, Germany), crystal violet dye content ≥90 % (Sigma), palladium(II) chloride (99.9% Aldrich), Rhodium(III) chloride hydrate(99.98% Aldrich), Ruthenium(III) chloride hydrate(99.98% Aldrich) and hexachloroplatinic acid hexahydrate (Alfa Aesar), have been used without further purifications.

Preparation of Metal Loaded TiO₂: Metal loaded TiO₂ was prepared by suspending 1.0 g of TiO₂ powder in 100 ml of deionized water by sonication for ten minutes, followed by the addition of the desired amount of prepared colloidal metal under continuous magnetic stirring. The reaction vessel was then irradiated with the light intensity of 2 mW.cm⁻² under inert environment by purging with argon gas over night [21]. After irradiation, the obtained powder was washed with deionized water several times and then dried overnight in an oven at 60 °C.

Characterization: X-ray diffraction (XRD) data for the Rietveld phase analysis of TiO₂ have been recorded on a Phillips PW1800 diffractometer using reflection geometry with variable divergence slits, Cu-Kα1, and a secondary monochromator. The phase analysis by the Rietveld method was carried out by using the TOPAS 2.0 (Bruker AXS) software. The average crystallite sizes of samples were quantitatively calculated using Scherrer formula after correcting the instrumental broadening.

All samples were degassed at 115 °C prior to nitrogen adsorption measurements. The Brunauer–Emmett–Teller (BET) surface area (SBET) of the powders was analyzed by nitrogen adsorption

using a Micromeritics ASAP 2020 nitrogen adsorption apparatus (USA). Micromeritics flow sorb. II 2300 GR nitrogen adsorption apparatus (USA). All measurements for the surface area were repeated three times and the average for these measurements was calculated.

UV–VIS diffused reflectance spectra of the samples were obtained for the dry-pressed film samples using a UV–VIS spectrophotometer (Varian Cary 100). Labsphere USRS-99–010 BaSO₄ was used as a reflectance standard in a UV–VIS diffuse reflectance experiment.

The surface morphologies of the films were investigated by a (NTMDT) Solver (P47-PRO) scanning probe microscope operating in the contact atomic force microscopy (AFM) mode with a scan speed of 1 Hz.

Adsorption Studies: Kinetic studies on the adsorption of CV dye by TiO₂ and M/TiO₂ were carried out in the dark, and it was found that adsorption equilibrium was achieved within 1 h (data not shown). Thus, 1 h was chosen as the adsorption equilibrium time. Batch equilibrium adsorption experiments were conducted in the dark over a range of initial concentrations [1-10 gm.L⁻¹], pH 6.0 with a fixed weight (0.15 g/100 ml) of the M/TiO₂ samples to obtain the adsorption isotherms of CV on the catalysts. The suspension was placed in 250 ml stoppered conical flasks and mechanically shaken at 120 rpm in a water bath shaker "Memmert WNB 22" at a constant temperature (25 °C). After reaching equilibrium, 3 cm³ of reaction mixture was collected and centrifuged (6000 rpm, 15 minutes) in a Hettich centrifuge. The supernatant was carefully collected in a syringe with a long pliable needle and centrifuged for a second time, at the same speed and for the same period of time. This second centrifugation was found necessary to remove the fine particles of TiO₂ that found effective on the result of analysis by uv-visible spectrophotometer. The amount of adsorbed dyes per gram TiO₂ at equilibrium, q_e (mg/g), was obtained by[22]

$$q_e = \frac{(C_0 - C_e)V}{W} \quad (7)$$

where C_0 and C_e (mg/L) are the initial and equilibrium concentrations of CV dye. V (L) is the volume of the solution, and W (g) is the weight of catalyst used.

Photocatalytic activity measurements: The photocatalytic experiments were conducted under ambient atmospheric conditions and at natural pH (6.0) using Philips mercury lamp UV (A) 365 nm, contains six lamps of 15 W for each one (Germany) as the light source, The incident photon flux (2 mW.cm⁻²) was determined by UV-meter (Dr.Honle). For each run, 0.3 g of Metals doping TiO₂ powders was dispersed in 200 mL of CV aqueous solution with a concentration of (0.5-10 mg.L⁻¹). Prior to the beginning of irradiation, the mixture was allowed to equilibrate in the dark with stirring for 60 minutes. at predominant times, 3 cm³ of reaction mixture was collected and centrifuged (6000 rpm, 15 minutes) in a Hettich centrifuge. The apparent kinetics of disappearance of the substrate, crystal violet dye, was determined by following the concentration of the substrate ($\lambda_{max} = 592$ nm) using a UV–visible spectrophotometer.

RESULTS AND DISCUSSION

Characterization

X-ray diffraction: X-ray diffraction (XRD) is considered one of most important properties affecting photocatalytic efficiency of TiO₂[23]. For TiO₂ (anatase type), the major peaks were observed at 2θ values of 25.3°, 48.2°, 55.0° and 62.6° which are assigned to (101), (200), (220), (211) and (204) reflections of anatase [24]. Figure 1 shows the XRD patterns of undoped TiO₂ and each M/TiO₂ samples, the results indicate that the doping of metals (Pt, Pd, Rh, and Ru) had no deleterious effect on the crystal phase of TiO₂[25]. May be two factors can cause this result, one is that the deposited metals " Pt, Pd, Rh, and Ru " are highly dispersed in the support matrix, the other is the percentage of metals are too low.[26]

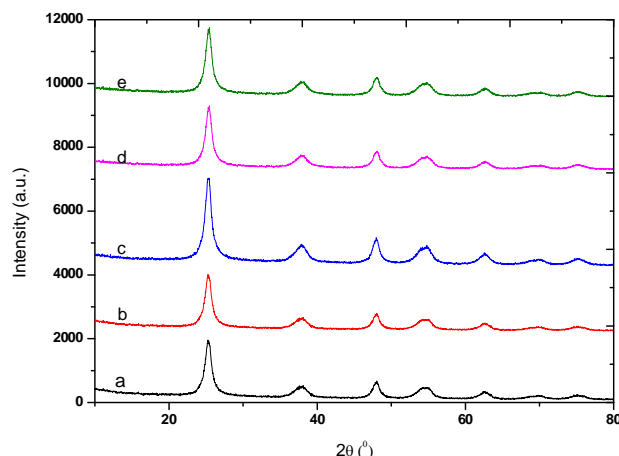


FIGURE 1: The XRD spectra of ((a) TiO₂; (b) Pt/TiO₂; (c) Pd/TiO₂; (d) Rh/TiO₂; (e) Ru/TiO₂).

The diffraction peak corresponding to 101 crystal plane of each sample was selected for calculating the crystal size by using the Scherrer equation (8). For the peak (101) reflection at 2θ (25.40) by using the full width at half maximum (fwhm) [27], the results are illustrated in Table 1.

TABLE 1. Physicochemical properties of undoped and Pt, Pd, Rh, and Ru doped titanium catalyst

Sample	Crystalline size ^a (nm)	Surface area ^b (m ² .g ⁻¹)	Average diameter ^c (nm)	Band gap ^d (e.v.)
TiO ₂	8.13	250	82.44	3.17
Pt/TiO ₂	8.21	223	59.55	3.16
Pd/TiO ₂	8.29	225	65.38	3.16
Rh/TiO ₂	8.70	200	76.11	3.12
Ru/TiO ₂	8.77	196	71.44	3.11

a Average crystallite size determined by XRD using the Scherrer equation.

b Specific surface area data calculated from the BET method.

c Average diameter calculated from the AFM method

d Band gap calculated from uv-visible absorbance by depending on Kubelka–Munk equation.

$$P = \frac{k\lambda}{\beta \cos\theta} \quad (8)$$

crystal size (P) can be estimated based on the peak width (B) giving a shape factor (k) of 0.9, λ (the wavelength of the CuK α 1 x-ray source) of 0.1541 nm, β (full peak width at half maximum corrected for instrumental broadening). It's clear (101) peak affecting by metals doping and caused decreasing its intensity, whose intensity decreases in the order of Pt, Pd, Rh and Ru, indicating that among them Ru-doping can most efficiently inhibit the surface of TiO₂ nanocrystallites.

Specific surface areas BET: Specific surface areas of the undoped TiO₂ and the M/TiO₂ samples with different doping elements were measured and the results are shown in Table 1. As shown in Table 1, the surface area strongly depends on the kind of metals doping. The surface area of the doping metals decreased as follow Pt/TiO₂, Pd/TiO₂, Rh/TiO₂ and Ru/TiO₂, this decreasing depend on the density of metals doping. The decrease in the crystallite size of doped samples leads to an increase in the surface area of the catalyst as compared to the undoped sample[28].

Diffuse Reflectance Spectra DRS: Figure 2 shows DRS spectra of the undoped TiO_2 and M/TiO_2 samples with optimal doping concentrations. The undoped TiO_2 was characterized with a sharp adsorption edge at about 390 nm indicating a band-gap of ≈ 3.17 eV [29]. The band gap energy (E_g) of these samples was estimated from the plot of square root of Kubelka-Munk function versus photon energy (Figure not shown). [30] The absorption band gap energies of all the samples are summarized in Table 1. It is obvious from Figure (2) the metal-loaded materials show small shifting in the value of wavelength characteristic absorption patterns due to the colouration of the powders. The shifting of absorption of visible light by metallised samples has been ascribed to low-energy transitions between thvalencebandof TiO_2 and localised energy levels introduced to the band-gap by deposited metal clusters [31].

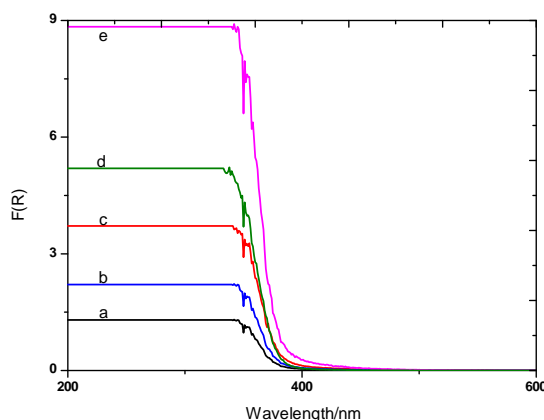
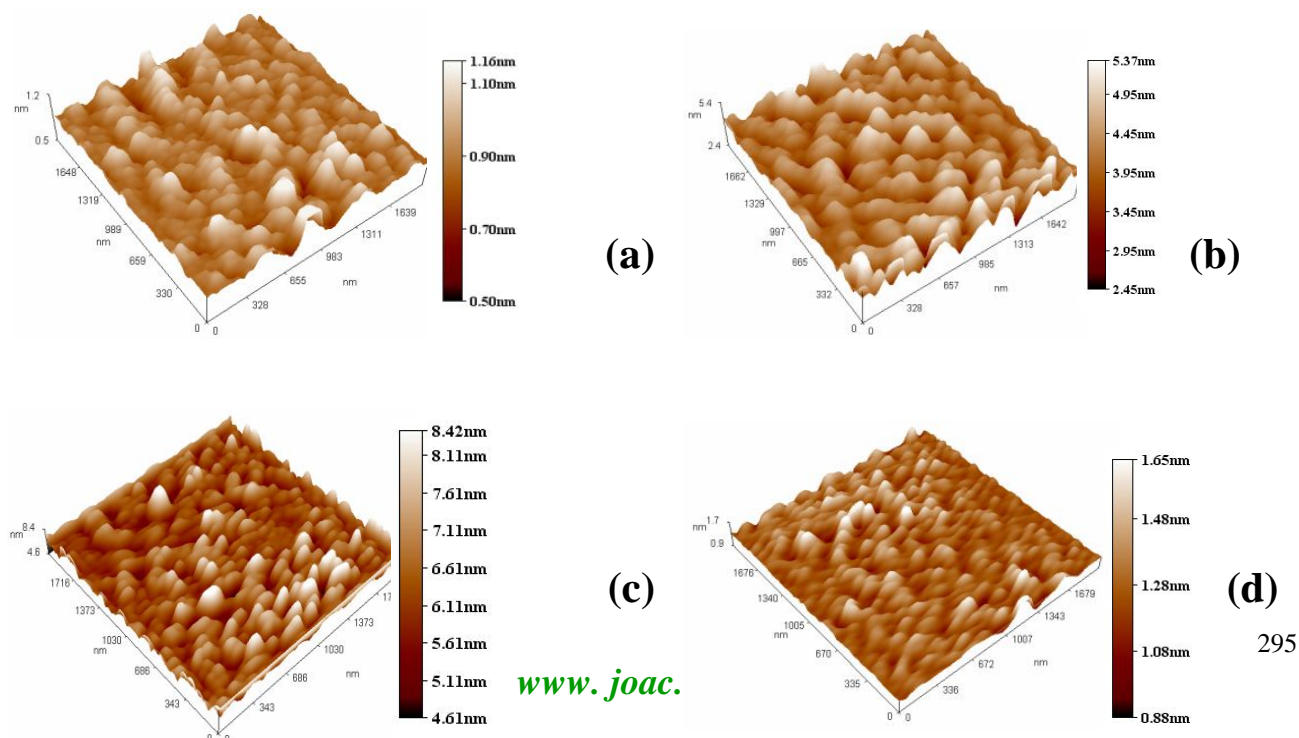


FIG 2: UV–vis diffuse reflectance spectra of ((a) TiO_2 ; (b) Pd/TiO_2 ; (c) Pt/TiO_2 ; (d) Rh/TiO_2 ; (e) Ru/TiO_2).

Atomic Force Microscopy AFM: Figure 3 displays typical AFM images of TiO_2 and M/TiO_2 films. It can be seen that these films are quite uniform. In compared with TiO_2 thin films, the surfaces grain sizes and the average surface roughness of M/TiO_2 ones decrease. The particle-size distributions of TiO_2 and metals doping on TiO_2 films in AFM images were about 55–82 nm, much greater than the crystallite sizes calculated from the XRD results. The increase in the crystallite sizes of TiO_2 particles in AFM results is due to the aggregation of the primary crystallites [32]. The surface roughness and the average diameter were observed to slightly affecting on addition of metals deposition as shown in Table 1.



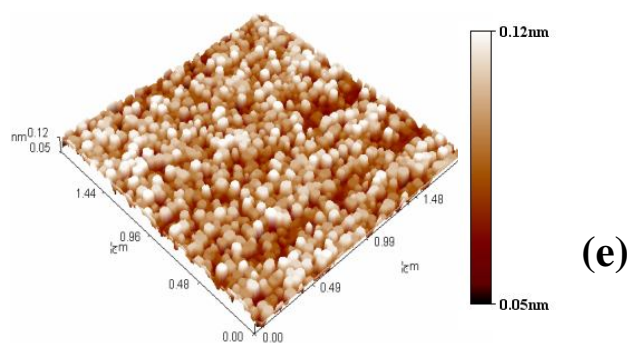


FIG 3: AFM images of ((a) TiO₂; (b) Pd/TiO₂; (c) Pt/TiO₂; (d) Rh/TiO₂; (e) Ru/TiO₂) thin film.

Adsorption Isotherms: Adsorption isotherms are important for the description of how adsorbate will interact with an adsorbent and are critical in optimizing the use of adsorbent. Thus, the correlation of experimental equilibrium data using either a theoretical or empirical equation is essential for adsorption data interpretation and prediction. Sorption isotherm is the relationship between concentration and adsorption capacity at each particular temperature. The equilibrium adsorption isotherm is of importance in the first step of adsorption/photocatalytic systems. The experimental equilibrium data for CV adsorption on metals/TiO₂, calculated from Eq. (7), are fitted with Langmuir[33], Freundlich[34] and Langmuir-Freundlich (Sips)[35] isotherms, Eqs. (8), (10) and (11), were presented in Figures 4-8. The calculated constants of the three isotherm equations along with R² values are presented in Table 2. Which were obtained by non-linear curve fitted plotted q_e versus C_e.

The theoretical Langmuir isotherm[33] assumes that adsorption occurs at specific homogeneous sites within the adsorbent and the capacity of the adsorbent is finite.

$$q_e = \frac{K_L q_m C_e}{1 + K_L C_e} \quad (8)$$

where C_e is the equilibrium concentration (mg L⁻¹); q_e is the amount of dye adsorbed at equilibrium (mg/g); q_m is q_e for a complete monolayer (mg/g), which gives the maximum adsorption capacity of adsorbent; and K_L is the sorption equilibrium constant (L mg⁻¹).

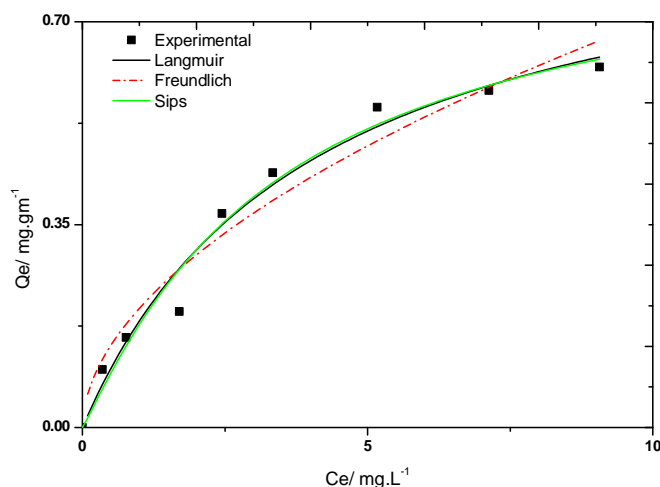


FIG 4: Adsorption isotherms for the adsorption of CV dye. pH: 6; T: 298 K, adsorbent dosage: TiO₂ (1.5 g.L⁻¹); contact time: 60 min; agitation speed: 200 rpm.

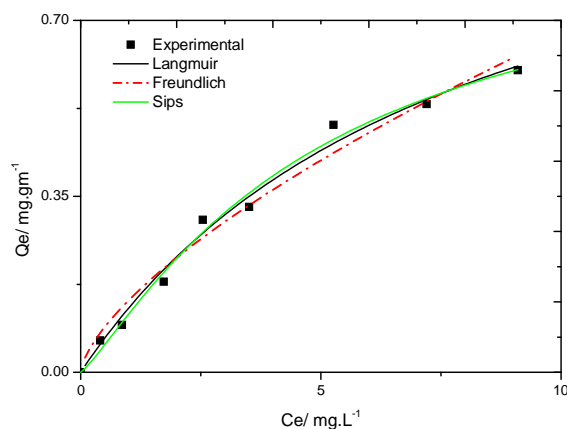


FIG 5: Adsorption isotherms for the adsorption of CV dye. pH: 6; T: 298 K, adsorbent dosage: Pt/TiO₂ (1.5 g.L⁻¹); contact time: 60 min; agitation speed: 200 rpm

The essential characteristics of the Langmuir isotherm can be expressed by a dimensionless constant called equilibrium parameter, R_L , that is defined by the following equation defined as[36].

$$R_L = \frac{1}{1 + K_L C_0} \quad (9)$$

where C_0 is the initial dye concentration. The nature of the adsorption process to be either unfavourable ($R_L > 1$), linear ($R_L = 1$), favourable ($0 < R_L < 1$) or irreversible ($R_L = 0$)[37].

From our study, R_L values for CV aqueous solution adsorption on M/TiO₂ as shown in Figure (9) ranged from 0.01 to 0.13. This is for initial concentration of (0.5–10 mg/L) of CV aqueous solution. Therefore, the adsorption process is favorable.

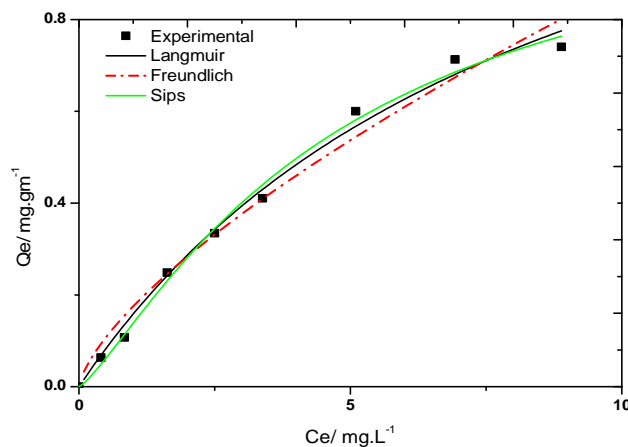


FIG 6: Adsorption isotherms for the adsorption of CV dye. pH: 6; T: 298 K, adsorbent dosage: Pd/TiO₂ (1.5 g.L⁻¹); contact time: 60 min; agitation speed: 200 rpm.

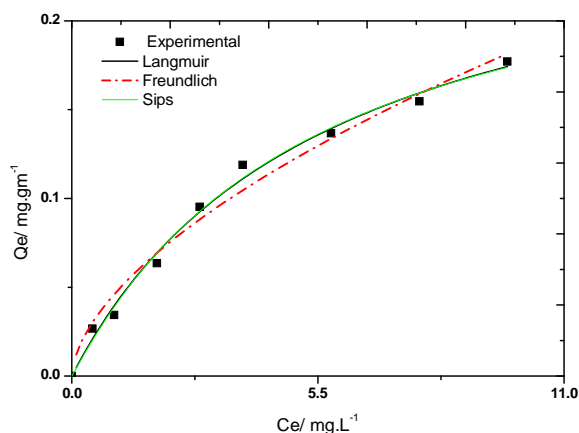


FIG 7: Adsorption isotherms for the adsorption of CV dye. pH: 6; T: 298 K, adsorbent dosage: Rh/TiO₂ (1.5 g.L⁻¹); contact time: 60 min; agitation speed: 200 rpm.

The Freundlich isotherm[34] is an empirical equation employed to describe heterogeneous systems. It does not indicate a finite uptake capacity of the adsorbent and can thus only be reasonably applied in the low to intermediate adsorbate concentration ranges. The Freundlich equation can be written as:

$$q_e = K_F C_e^{1/n} \quad (10)$$

Where K_F ((mg/g) (L/mg)^{1/n}) and n are Freundlich constants which give a measure of adsorption capacity and adsorption intensity, respectively.

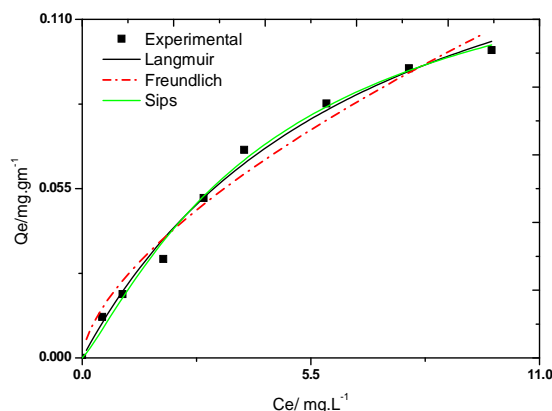


FIG 8: Adsorption isotherms for the adsorption of CV dye. pH: 6; T: 298 K, adsorbent dosage: Ru/TiO₂ (1.5 g.L⁻¹); contact time: 60 min; agitation speed: 200 rpm

Sips isotherm model[35] is a combination of the Langmuir and Freundlich isotherm type models and expected to describe heterogeneous surface much better. At low adsorbate concentrations, the Sips isotherm approaches the Freundlich isotherm, whereas it approaches the Langmuir isotherm at high concentrations. The model can be written as:

$$q_e = \frac{q_m K_S C_e^{1/m}}{1 + K_S C_e^{1/m}} \quad (11)$$

Where q_m (mg.g⁻¹) is the maximum amount of CV adsorbed per unit mass of M/TiO₂, K_S (L.mg⁻¹)^{1/m} is Sips constant related to energy of adsorption, and parameter m is the Sips exponent (non-dimensional) could be regarded as the parameter characterizing the system heterogeneity. A comparison of the coefficients of determination for the three isotherms was conducted and listed in Table 2. The coefficients

of determination, R^2 , were between 0.96585 to 0.989 for the Langmuir isotherm, 0.9389 to 0.97402 for the Freundlich isotherm, while for the Sips isotherm they were between 0.97317 to 0.99309 indicating that the all models give good obeying for adsorption of crystal violet dye on metals doping TiO_2 surface, but in order of Sips > Langmuir > Freundlich. The results revealed that the equilibrium data are fitted by the three-parameter model rather than the two-parameter models. This may be due to the ability of Sips isotherm to predict wide adsorbate concentration ranges.

Photocatalytic activity measurements: The photocatalytic activities of the TiO_2 and metals doping samples are evaluated by the degradation of CV in the aqueous solution under UV light irradiation. The changes in the concentration of CV recorded during irradiation at specific time intervals are shown in Figure 10.

TABLE 2: Isotherm parameters and regression data for crystal violet dye sorption on (TiO_2 ; Pd/ TiO_2 ; Pt/ TiO_2 ; Rh/ TiO_2 ; and Ru/ TiO_2) at 25 °C and pH 6.

Isotherm	Surface Parameters	TiO_2	Pt/ TiO_2	Pd/ TiO_2	Rh/ TiO_2	Ru/ TiO_2
		value	value	value	value	value
Langmuir	$q_m(\text{mg}\cdot\text{g}^{-1})$	0.92161	1.13921	1.53224	0.27549	0.17467
	$K_L(\text{L}\cdot\text{mg}^{-1})$	0.2494	0.12636	0.11532	0.17679	0.14533
	R^2	0.96585	0.98559	0.98861	0.989	0.98817
Freundlich	$K_F((\text{L}\cdot\text{mg}^{-1})(\text{L}\cdot\text{mg}^{-1})^{1/n})$	0.20583	0.14317	0.17524	0.04747	0.02552
	N	0.53369	0.67112	0.69587	0.58943	0.62528
	R^2	0.9389	0.97036	0.97184	0.97402	0.9685
Sips	$q_m(\text{mg}\cdot\text{g}^{-1})$	0.85451	0.89165	1.10954	0.26627	0.14403
	$K_S((\text{L}\cdot\text{mg}^{-1})^{1/m})$	0.26322	0.14933	0.14268	0.18134	0.1625
	M	1.08875	1.19218	1.25392	1.02815	1.17767
	R^2	0.97317	0.98922	0.99309	0.99118	0.99171

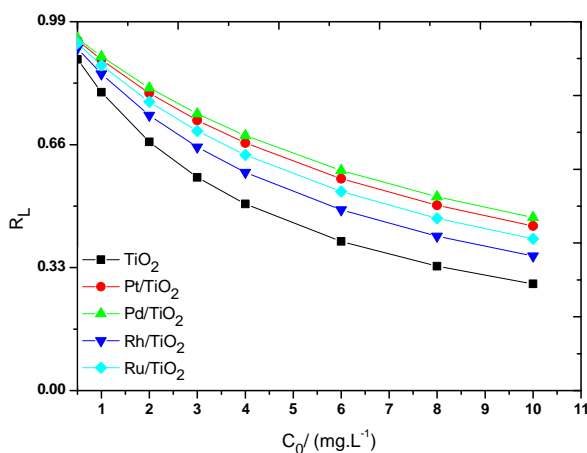


FIG 9: Dimensionless separation factor, R_L for adsorbent catalysis surfaces (TiO_2 and M/ TiO_2) in the presence of different initial concentrations crystal violet dye.

Figure 10 shows that the photolysis of CV can be negligible. Moreover, the concentration of CV does not change in observed case in the presence of the catalysts under dark condition. Therefore, the presence of both UV light and photocatalyst is necessary for the photocatalytic reaction to proceed. The observed results reveal that the order of photocatalytic activity of metal-doped TiO₂ depends on two important factors such as electron affinity of the metal and suitable work function to form a favourable contact with the TiO₂ semiconductor. The photocatalytic activity of Pt/TiO₂ and Pd/TiO₂ is higher than Rh/TiO₂ and Ru/TiO₂ due to their high electron affinity behaviour[38] and suitable work function[39].

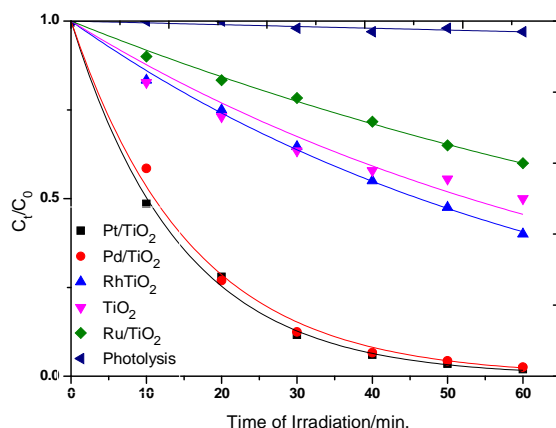


FIG 10: Photocatalytic degradation of CV dye [3 mg.L⁻¹] represented by C_t/C_0 via photolysis with or without catalyst at an initial pH level of 6.01, air flow rate 10 ml.s⁻¹, L.I. (mW.cm⁻²), T: 298 K with catalyst dosage of 1.5 g.L⁻¹.

The weak photocatalytic activity of degradation may be either due to weak electron trapping capability of Rh, and Ru metals when compared to Pt or Pd or to the fact that a large fraction of Rh, and Ru particles are non-metallic[40]. It is important both from an application and a mechanistic from point of view to study the dependence of the photocatalytic reaction rate on the substrate concentration. Several experimental results indicated that the destruction rates of photocatalytic oxidation of various dyes over illuminated TiO₂ and M/TiO₂ fitted the Langmuir–Hinshelwood (L–H) kinetics model [41, 42]:

$$r = \frac{dC}{dt} = \frac{k_L K_{ads} C_0}{1 + K_{ads} C_0} \quad (12)$$

where r is the oxidation rate of the reactant (mg/l min), C_0 the initial concentration of the reactant (mg/l), t the illumination time, k_L the reaction rate constant (mg/l min), and K_{ads} is the adsorption coefficient of the reactant (l/mg), Figure 11 shows the L-H model in the presence of different metals doped on TiO₂ surface, it is clear all metals doped give good agreements for L-H kinetic model.

It is generally noted that the degradation rate increases with the increase in dye concentration to a certain level and a further increase in dye concentration leads to decrease the degradation rate of the dye[43].

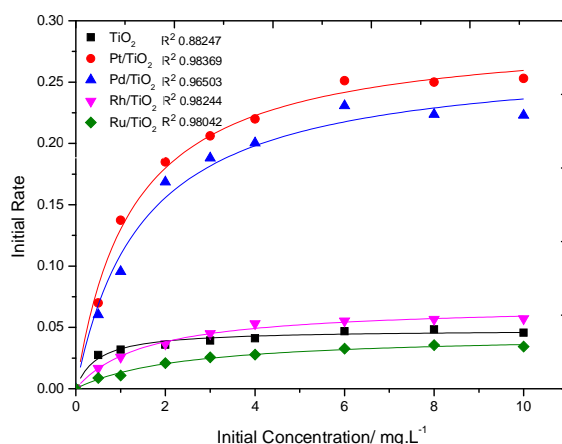


FIG 11: Effect of initial CV dye concentration on photodegradation: catalyst suspended = 1.5 g.L^{-1} ; pH 6; T: 298 K, air flow rate = 10 mL s^{-1} ; irradiation time (degradation = 40 min); L.I. 2 mW.cm^{-2} .

The rate of degradation relates to the probability of $\cdot\text{OH}$ radicals formation on the catalyst surface and to the probability of $\cdot\text{OH}$ radicals reacting with dye molecules. As the initial concentrations of the dye increase the probability of reaction between dye molecules and oxidizing species also increases, leading to an enhancement in the decolorization rate. On the contrary, the degradation efficiency of the dye decreases as the dye concentration increases further. At a high dye concentration, a significant amount of UV may be absorbed by the dye molecules rather than the TiO_2 particles and that reduces the efficiency of the catalytic reaction because the concentrations of OH^\cdot and $\text{O}_2^{\cdot-}$ decrease [41, 44]. Reaction rate constant, and the adsorption coefficient of the reactant which determined non-linear fitting curve are showing in Figure 12, it was obvious from Figure 12, the adsorption constants values give accepted behavior of a results that obtained from adsorption isotherms studying except of TiO_2 surface.

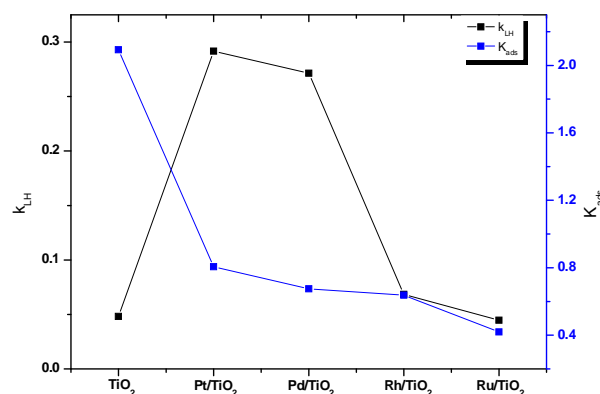


FIG 12: Dependence of parameters constants of Langmuir-Hinshelwood model (k_{LH} and K_{ads}) on the catalyst type (bare TiO_2 , Pt/TiO_2 , Pd/TiO_2 , Rh/TiO_2 , and Ru/TiO_2).

APPLICATIONS

The adsorption and photocatalytic degradation of crystal violet dye over bare TiO_2 , Pt/TiO_2 , Pd/TiO_2 , Rh/TiO_2 and Ru/TiO_2 , has been studied. The addition of Pd or Pt dramatically increases the adsorption and photocatalytic degradation of CV dye. On the contrary, the Rh doped TiO_2 is far less active, while Ru doped TiO_2 decrease the photocatalytic activity of CV.

CONCLUSIONS

Various metals were doping on TiO₂ surface by a photodeposition method. Adsorption of CV dye in the presence of TiO₂ and M/TiO₂ exhibit accepted behaviour. The isotherm models Langmuir, Freundlich, Sips were analyzed to describe the adsorption behavior of M/TiO₂. The experimental data was better fitted with the Sips adsorption model. The kinetics of photocatalytic degradation under UV light of TiO₂ and M/TiO₂ has been investigated. Langmuir–Hinshelwood kinetics were observed under UV light. Both Pd and Pt deposited on TiO₂ show a strong photocatalytic activity. On the contrary, Rh/TiO₂ does not enhance photocatalytic activity while Ru/TiO₂ does appear to be as inactive.

ACKNOWLEDGEMENTS

We gratefully acknowledge support of the chemistry department, Faculty of girls' sciences, Babylon university, Ministry of higher education and scientific research, Iraq.

REFERENCES

- [1] R. Jain and S. Sikarwar, *Environmental Technology*, **2010**, 31, 1403-1410.
- [2] P. Bansal, and D. Sud *Desalination*, **2011**, 267, 244-249.
- [3] A. Mittal, J. Mittal, A. Malviya, D. Kaur, and V. K. Gupta, *Journal of Colloid and Interface Science*, **2010**, 343, 463-473.
- [4] R. Ahmad, *J. Hazard. Mater*, **2009**, 171, 767-773.
- [5] F. Guzman-Duque, C. Pétrier, C. Pulgarin, G. Peñuela, and R. A. Torres-Palma, *Ultrasonics Sonochemistry*, **2011**, 18, 440-446.
- [6] G. Ovejero, A. Rodríguez, A. Vallet, and J. García, *Applied Catalysis B: Environmental*, **2012**, 125, 166-171.
- [7] Y. Cheng, H. Lin, Z. Chen, M. Megharaj and R. Naidu, *Ecotoxicology and Environmental Safety*, **2012**, 83, 108-114.
- [8] Y. B. Liao, J. X. Wang, J. Lin, W. Chung, W. Lin, and C. Chen, *Catalysis Today*, **2011**, 174, 148-159.
- [9] A.K. Gupta, A. Pal, and C. Sahoo, *Dyes and Pigments*, **2006**, 69, 224-232.
- [10] A. Nezamzadeh-Ejhieh, and Z. Banan, *Desalination*, **2012**, 284, 157-166.
- [11] H. Fan, S. Huang, W. Chung, J. Jan, W. Lin, and C. Chen, *Journal of Hazardous Materials*, **2009**, 171, 1032-1044.
- [12] S. P. Devipriya, Suguna Yesodharan, and E. P. Yesodharan, *International Journal of Photoenergy*, **2012**, 2012, 1-8.
- [13] A. Mahyar, M.A. Behnajady and N. Modirshahla, *Photochemistry and Photobiology*, **2011**, 87, 795–801.
- [14] I. K. Konstantinou, and T. A. Albanis, *Applied Catalysis B-Environmental*, **2003**, 42, 319-335.
- [15] M. R. Hoffmann, S.T. Martin, W. Choi and D. W. Bahnemann, *Chemical Reviews*, **1995**, 95, 69-96
- [16] M. Qamar, M. Saqui and M. Muneer, *Dyes and Pigments*, **2005**, 65, 1-9.
- [17] C. H. Wu, *Chemosphere*, **2004**, 57, 601-608.
- [18] B. Sun, P.G. Smirniotis and P. Boolchand, *Langmuir*, **2005**, 21, 11397–11403.
- [19] D. Hufschmidt, D. Bahnemann, J. J. Testab, C.A. Emilio and M. I. Litter, *Journal of Photochemistry and Photobiology A: Chemistry*, **2002**, 148, 223-231.
- [20] V.M. Menéndez-Flores, D. Friedmann and D. W. Bahnemann, *International Journal of Photoenergy*, **2008**, Article ID 280513, 11 pages, 2008. doi:10.1155/2008/280513.
- [21] A.A. Ismail, D.W. Bahnemann, L. Robben, V. Yarovy and M. Wark, *Chemistry of Materials*, **2010**, 22, 108–116.

- [22] N.Bao, Yuan Li, Z. Wei, G. Yin and J. Niu, *The Journal of Physical Chemistry C*, **2011**, 115, 5708–5719.
- [23] H. Zhao, S. Bennici, J. Shen and A. Auroux, *Applied Catalysis A: General*, **2009**, 356, 121-128.
- [24] Y. Cao, H. Tan, T. Shi, T. Tang, and J. Li, *Journal of Chemical Technology and Biotechnology* **2008**, 83, 546-552.
- [25] J. Zhang, L. Li and G. Li, *International Journal of Photoenergy*, **2012**, 2012, 1-7.
- [26] J. B. Zhong, Y. Lu, W. D. Jiang, Q. M. Meng, X. Y. He, J. Z. Li and Y. Q. Chen, *Journal of Hazardous Materials*, **2009**, 168, 1632-1635.
- [27] A.A. Ismail, D. W. Bahnemann, I. Bannat and M. Wark, *Journal of Physical Chemistry C*, **2009**, 113, 7429–7435.
- [28] A. Bokare, A. Sanap, M. Pai, S. Sabharwal and A. A. Athawale, *Colloids and Surfaces B: Biointerfaces*, **2013**, 102, 273– 280.
- [29] C. Bauer, P. Jacques and A. Kalt, *Journal of Photochemistry and Photobiology A: Chemistry*, **2001**, 140, 87-92.
- [30] N. Serpone, D. Lawless and R. Khairutdinov, *The Journal of Physical Chemistry*, **1995**, 99, 16646-16654.
- [31] S. Sakthivel, M. Shankar, M. Palanichamy, B. Arabindoo, D. W. Bahnemann and V. Murugesan *Water Research*, **2004**, 38, 3001-3008.
- [32] M. H. Ahmed, T.E. Keyes, J. A. Byrne, C. W. Blackledge and J. W. Hamilton, *Photochemistry and Photobiology A: Chemistry*, **2011**, 222, 123-131.
- [33] I. Langmuir, *Journal of American Chemical Society*, **1916**, 38, 2221-2295.
- [34] H.M. Freundlich, *Zeitschrift für Physikalische Chemie*, **1906**, 57A, 385-470.
- [35] R. Sips, *The Journal of Chemical Physics*, **1948**, 16, 490-495.
- [36] K. R. Hall, L. C. Eagleton, A. Acrivos and T. Vermeulen, *Industrial & Engineering Chemistry Fundamentals*, **1966**, 5, 212-223.
- [37] S. K. Das, J. Bhowal, A. R. Das and A. K. Guha, *Langmuir*, **2006**, 22, 7265-7272.
- [38] B. Lee, S. Kim, S. Lee, H. Lee and S. Choung, *International Journal of Photoenergy*, **2003**, 5, 21-25.
- [39] T.M Miller, *Behavioral Science*, **1993**, 38, 10–18.
- [40] Y.Z. Yanga, C.H. Changa and H. Idriss, *Applied Catalysis B: Environmental*, **2006**, 67, 217-222.
- [41] W.Z.Tang and H. An, *Chemosphere*, **1995**, 31, 4171-4183.
- [42] S. Senthilkumaar and K. Porkodi, *Journal of Colloid and Interface Science*, **2005**, 288, 184-189.
- [43] S. Sakthivel, B. Neppolian, M. V. Shankar, B. Arabindoo, M. Palanichamy and V. Murugesan, *Solar Energy Materials and Solar Cells*, **2003**, 77, 65-82.
- [44] C.M.So, M.Y. Cheng, J.C. Yu and P.K. Wong, *Chemosphere.*, **2002**, 46, 905-912.